Asian Journal of Chemistry; Vol. 32, No. 9 (2020), 2356-2364

ASIAN JOURNAL OF CHEMISTRY

https://doi.org/10.14233/ajchem.2020.22746

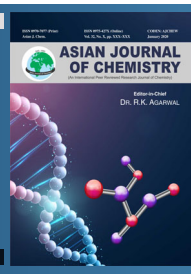

Spectral Characterization, Thermal and Antimicrobial Studies of Some Divalent Metal Chelates of 7-((3-Phenyl-4,5-dihydroisoxazol-5-yl)methyl)quinolin-8-ol

ASMA A. ALOTHMAN*, MUNIRAH D. ALBAQAMI and RAZAN A. ALSHGARI

Department of Chemistry, College of Science, King Saud University, P.O. Box 22452, Riyadh 11495, Saudi Arabia

*Corresponding author: E-mail: aaalothman@ksu.edu.sa

Received: 28 March 2020; *Accepted*: 30 June 2020; *Published online*: 20 August 2020; AJC-20038

A series of Cu(II), Ni(II) and Co(II) azo chelates (**AZC1-AZC3**) of 7-((3-phenyl-4,5-dihydroisoxazol-5-yl)methyl)quinolin-8-ol have been designed and obtained. Thermal measurements, molar conductance, magnetic moment, elemental analyses, spectral (IR, UV-Vis, ^{1}H and ^{13}C NMR, ESR, mass) were used to characterize insulated solid complexes. The metal complexes were assumed to be non-electrolytic by molar conductance values. Thermal properties and decomposition kinetics of the metal chelates are investigated using Coats-Redfern method. The kinetic parameters like activation energy (E*), pre-exponential factor (A) and entropy of activation (ΔS*) were quantified. Results of spectral studies of mass and TGA data confirmed the octahedral geometry for all chelates. Finally, the synthesized metal-complexes were tested for their *in vitro* antimicrobial efficacy.

Keywords: Azo dye chelates, DFT, Antimicrobial efficacy.

INTRODUCTION

Metalloazo dyes are highly versatile coordination compounds with a wide range of applications [1-5]. Well defined geometries, which can easily interact with biomolecules show that heteroaromatic moiety on combination with a positive charged metal center leads to metal complexes [6]. A number of compounds of naphthofuran derivatives are endowed with various biolo-gical activities like anthelmintic, anticonvulsant and antipyretic [7] and their plant extracts are being used for traditional medicines [8], while mansonone D and dunnione [9] of naphthofuran family are vital biologically active agents. In addition, naphtho-furans condensed with various heterocycles exhibited wide spectrum of activities [10]. The presence of oxygen and nitrogen donor atoms in the complexes shows significant antibacterial and anticancer activities [11,12].

Smaller size and higher nuclear charge of the metals like cobalt, nickel and copper to have great affinity for coordination. As much we know there is no work that has been reported on the synthesis of metal complexes of azo-dye derived from 7-((3-phenyl-4,5-dihydroisoxazol-5-yl)methyl)quinolin-8-ol and *p*-toluidine. The structural characterization was achieved applying the alternative analytical and spectral tools. The biological studies of azo dye and its metal chelates have been evaluated by screening their capability to inhibit the growth of some bacterial and fungi strains in addition to anticancer activity evaluation against HEPG2 cell line.

EXPERIMENTAL

A complexometric titration, is used to find the concentration of metal ions [13,14]. Spectra were recorded from 4000 to 400 cm^{-1} with 64 scans and resolution of 4 cm^{-1}. The ^{1}H NMR spectrum of samples was recorded in a Bruker Avance III 600 MHz (14 T) spectrometer. The samples were analyzed in a DMSO-d_6 solution and the chemical shifts were given relative to tetramethyl silane. The ^{13}C solid state NMR (SSNMR) spectra were recorded in a Bruker 300MHz spectrometer, using the combination of cross-polarization, proton decoupling and magic angle spinning (CP/MAS) at 10 kHz. Electrospray ionization mass spectrometry (ESI-MS) measurements were carried out using a Waters Quattro Micro API. Samples were evaluated in the positive mode. Using a CON 6000 conductivity meter molar conductivities were measured in DMSO solution of the complexes (10^{-3} M), Cyberscan, Eutech instruments. The operative magnetic moments were calculated using the relation μ_{eff} =

2.828 $(\lambda_m T)^{1/2}$ B.M., where λ_m is the molar magnetic susceptibility adjusted for diamagnetism of all atoms in the compounds using Selwood and Pascal's constants. The X-band EPR spectrum was performed at LNT (77 K) using TCNE as the g-marker. Thermal analysis (TG/DTG) was attained out by using a Shimadzu DTA/TG-50. Thermal analyzer with a heating rate of 10 ºC /min in nitrogen atmosphere with a following rate 20 mL/min in the temperature range 30-900 ºC using platinum crucibles.

Synthesis of ligand (AZ): *p*-Toluidine was coupled to 7-((3-phenyl-4,5-dihydroisoxazol-5-yl)methyl)quinolin-8-ol according to the reported procedure [15] to yield the azo dye ligand 7-((3-phenyl-4,5-dihydroisoxazol-5-yl)methyl)-5-(*p*-tolyldiazenyl)quinolin-8-ol (Fig. 1). In this method, *p*-toluidine (1.07 g, 0.01 mol) was dissolved in acidic distilled water (10 mL of water containing 1.47 mL of 12 M (0.03 mol) conc. HCl. The temperature of the obtained solution was decreased to -5 ºC while stirring. A cold solution containing 0.689 g (0.01 mol) of $NaNO_2$ was poured dropwise into this solution to form diazonium chloride. The obtained solution was then slowly poured into NaOH solution (0.01 mol) containing 3.04 g of 7-((3-phenyl-4,5-dihydroisoxazol-5-yl)methyl)quinolin-8-ol. The coloured product, which started to appear during addition, was preserved in an ice bath with stirring for 2 h. The precipitate was then separated by filtration, rinsed with deionized water and finally dried in a vacuum desiccator over anhydrous calcium chloride.

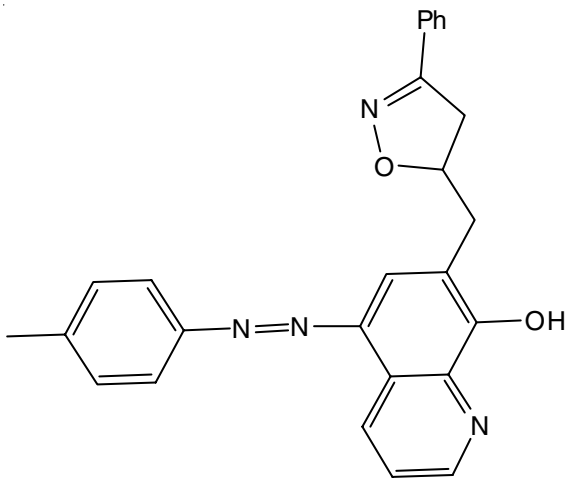

Fig. 1. Structure of **AZ** [7-((3-phenyl-4,5-dihydroisoxazol-5-yl)methyl)-5-(*p*-tolyldiazenyl)quinolin-8-ol]

Synthesis of metal complexes: To a hot stirred solution of an appropriate ligand (2 mmol) in ethanol (15 mL) was added the solution of metal(II) chloride (1 mmol) made in warm ethanol (10 mL) and the resultant mixture refluxed for 3 h. The solid formed during refluxing or upon cooling was collected by suction filtration. Thorough washing with hot ethanol followed by ether or recrystallization from aqueous ethanol gave purified products (Fig. 2).

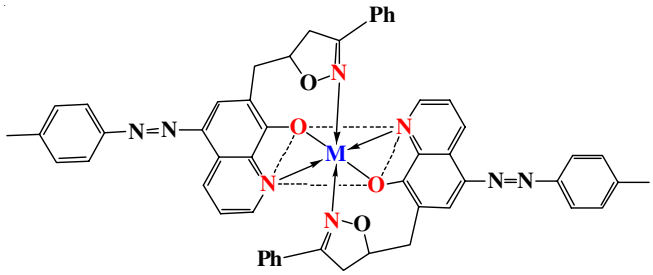

M = Cu(II), Co(II) and Ni(II)

Fig. 2. Suggested structure of azo-dye Cu(II) Co(II) and Ni(II) complexes

Biological activity: Antimicrobial were determined using disc-agar diffusion method [16] at micro analytical unit (Cairo University) against *Escherichia coli* as Gram-negative bacteria, *Staphylococcus aureus* as Gram-positive bacteria, *Aspergillus flavus* and *Candida albicans* as fungi. Calibrant discs of tetracycline (antibacterial substance), amphotericin B (antifungal substance) conducted as positive controls for antimicrobial efficacy. Filter discs immersed in 10 µL of dimethyl sulfoxide have been applied as a negative control. Shortly, 100 µL of the test bacteria/fungi has been grown in 10 mL of freshly prepared media until they reached a count of approximately 10^8 cells/mL for bacteria or 10^5 cells/mL for fungi. Microbial suspension (100 µL) has been diffused onto agar dishes. Dishes incubated with *Aspergillus flavus* at 25 ºC for 48 h; *Staphylococcus aureus* and *Escherichia coli* incubated at 35-37 ºC for 24-48 h and *Candida albicans* incubated at 30 ºC for 24-48 h. Then, the diameters of the inhibition zones have been recorded.

RESULTS AND DISCUSSION

The ligand and its metal complexes were subjected to elemental analysis (Table-1) and the data obtained agreed well with the assigned formulae of the proposed structure. The general formula of the metal complexes can be represented as $[M(AZ)_2]$; (M = Cu^{2+}, Ni^{2+} and Co^{2+} where AZ is azo-dye ligand).

TABLE 1
ANALYTICAL DATA OF THE LIGAND (AZ) AND THEIR METAL COMPLEXES (**AZ1-AZ3**)

Compound (m.f.)	m.w. found (calcd.)	m.p. (°C)	Colour (Yield, %)	Elemental analyses (%): Found (calcd.)				μ_{eff} at 298 (BM)
				C	H	N	M	
Ligand	408	120-122	Faint yellow	73.51	4.91	13.65	–	–
$C_{25}H_{20}N_4O_2$	(405.5)		(84.3)	(73.51)	(4.94)	(13.72)		
$[Cu(AZ)_2]$	906	258	Faint brown	68.76	4.67	12.36	7.00	3.92
$C_{52}H_{42}N_8O_4Cu$	(906.5)		(63.8)	(68.90)	(4.57)	(12.32)	(7.01)	
$[Ni(AZ)_2]$	901	246	Blue	69.22	4.63	12.38	6.43	2.89
$C_{52}H_{42}N_8O_4Ni$	(901.7)		(47.8)	(69.27)	(4.70)	(12.43)	(6.51)	
$[Co(AZ)_2]$	902	246	Dark blue	69.18	4.86	12.34	6.47	1.83
$C_{52}H_{42}N_8O_4Co$	(901.9)		(52.4)	(69.25)	(4.69)	(12.42)	(6.53)	

The ESI mass spectrum of ligand (Fig. 3) displays the prominent molecular ion peak (M^+) at *m/z* = 408.5. The base peak is appeared at *m/z* = 197 due to $C_{12}H_7NO_2^+$ ion. The other fragments give the peaks at 58, 64, 83, 92, 115, 128, 155, 167, 178, 213, 240 and 273 amu with various intensities. The mass spectra of Cu(II), Ni(II) and Co(II) complexes displayed molecular peaks at *m/z* (%) 906.5 (28.45 %), 901.7 (24.96 %) and 901.9 (23.62 %), respectively, suggested that the molecular weights of the assigned products matched with elemental analyses.

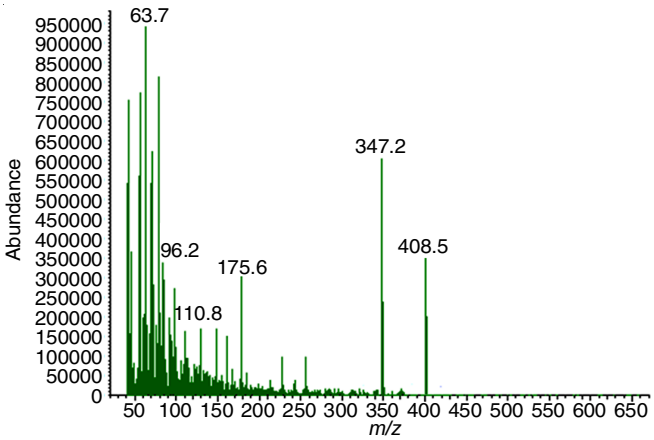

Fig. 3. Mass spectrum of **AZ**

Molar conductivity: The molar conductivities of **AZ1-AZ3** were measured after the metal complexes were dissolved in DMF. The values of the molar conductivity for azo-dye complexes (**AZ1-AZ3**) were found in the range (11.37-18.82 Ω^{-1} cm^2 mol^{-1}). According to Geary [17], the values implied that the complexes are non-electrolytic in nature.

IR analysis: In comparison to parent ligand and azo complexes (**AZC1-AZC3**), the main moieties like isoxazole and 8-hydroxyquinoline nitrogen (-C=N) and phenol oxygen (-OH) can be distinguished with metal complexes (Table-2). The band at 1592 cm^{-1} assigned to ν(C=N) linkage confirm the formation of azo dye (**AZ**) [18]. The stretching frequency observed at 2857 cm^{-1} in 7-((3-phenyl-4,5-dihydroisoxazol-5-yl)methyl)-5-(phenyldiazenyl)quinolin-8-ol displays the presence of O–H···N intermolecular hydrogen bonding and a strong band at 1218 cm^{-1} possesses highest percentage of enol-imino tautomer due to the stabilization of phenolic C-O bond. Similarly, a band at 1198 cm^{-1} corresponds ν(C-O-C) stretching vibrations of the isoxazole ring [19]. In the IR spectra of synthesized metal complexes, it was seen that band comparing to ν(C=N) bunch movements to bring down side by 18-26 cm^{-1}, which shows a bond is framed between azomethine nitrogen and metal complex [18]. The band in the range of 1587-1577 cm^{-1} in the IR spectra of metal complexes **AZ1-AZ3** relates to ν(HC=N) assembly. The same is supported by the proximity of band related to ν(M-N) bond in the range of 447-424 cm^{-1}. The wide band related to ν(-OH) vibrations at 3238 cm^{-1} in the ligand disappeared after complexes formation due to the deprotonation of phenol -OH within the complexes formation [20]. No band identified with ν(O-H) stretching vibrations was seen in the IR spectra of metal complexes, which shows the deprotonation of the enol group and synchronize of enol oxygen to metal ions [19]. A reappearance of ν(C-O) in the IR spectra of metal complexes at lower range around 673-669 cm^{-1} also confirmed the formation of metal complexes [18]. Moreover, presence of new band due to ν(M-O) bond in the range of 538-516 cm^{-1} [21] also affirmed the formation of the metal complexes. The ν(C-O-C) mode of furan ring in the uncoordinated Schiff base remains unchanged in the spectra of their respective complexes. This suggests that the oxygen ring did not participate in coordination. The correlation of IR spectra of ligand and its metal complexes suggested the tridentate nature of the synthesized ligand AZ, which coordinates through isoxazole, 8-hydroxyquinoline nitrogen and oxygen of phenol groups.

NMR analysis: The ^1H & ^{13}C NMR analysis of 7-((3-phenyl-4-5-dihydroisoxazol-5-yl)methyl)-5-(phenyldiazenyl)quinolin-8-ol (**AZ**) had been performed in DMSO. In ^1H NMR spectra, appearance of a singlet at δ 11.5 ppm, affirms the formation of azo-dye ligand **AZ** (Fig. 4), was assigned to hydroxyl group (-OH) proton. The protons of two -CH_2 group showed at multipets at δ 3.0 and 3.6 ppm. In ^{13}C NMR (Fig. 5), (-C=N) isoxazole ring carbon showed signal at δ 165 ppm, (-C=N-) 8-hydroxy-

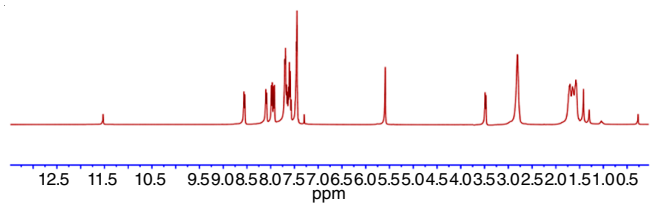

Fig. 4. ^1H NMR spectrum of **AZ**

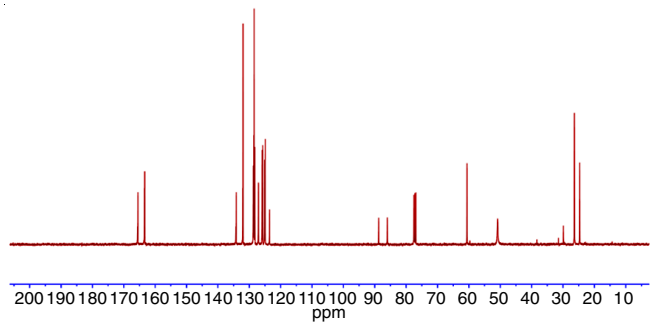

Fig. 5. ^{13}C NMR spectrum of **AZ**

TABLE-2
IMPORTANT INFRARED SPECTRAL BANDS (cm^{-1}) OF THE LIGAND (**AZ**) AND THEIR METAL COMPLEXES (**AZ1-AZ3**)

Compd.	ν(OH)	ν(C=N)	ν(C–O)	ν(C–O–C)	ν(M–O)	ν(M–N)
AZ	3238br	1592m	1218m	1198m	–	–
AZ1	–	1580m	1202m	1197m	523m	424m
AZ2	–	1580sh	1203s	1194m	516m	436m
AZ3	–	1578m	1202m	1197m	538s	447s

quinoline ring carbon at 162 ppm, (-C-O) isoxazole ring carbon at 161.47 ppm, (C-O) 8-hydroxyquinoline ring at 154 ppm, (-CH_2-) isoxazole ring and (-CH_2-) aliphatic group at 41.0 and 38.4 ppm, respectively. The chemical shift of characteristic of ^{1}H & ^{13}C NMR in DMSO-d_6 of Schiff base ligand is shown in Fig. 6.

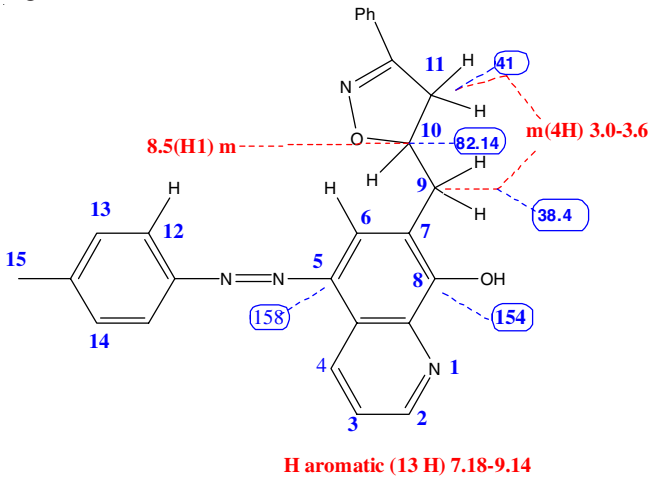

Fig. 6. Chemical shift of characteristic of NMR ^{1}H and ^{13}C in DMSO-d_6 of ligand

Electronic spectra and magnetic moment measurements: The electronic spectra of ligand and its metal complexes were recorded in DMF arrangement in the range of 200-700 nm (Fig. 7a-d). In the UV-visible spectra of azo-dye ligand (AZ), two high force retention groups were shown at 36,432 and 27,628 cm^{-1} which were transferable to intra-ligand π-π* and n-π* transitions [21]. These transitions were also seen in the spectra of the complexes, yet moved to longer wavelength, affirmed the coordination of the ligand to metal(II) complexes.

The electronic spectrum of Co(II) complex displays three bands at 10,869, 15,114 and 24,827 cm^{-1}, which are assigned to $^4T_{1g} \rightarrow {}^4T_{2g}(F)(\nu_1)$, $^4T_{1g} \rightarrow {}^4A_{2g}(F)(\nu_2)$ and $^4T_{1g} \rightarrow {}^4T_{1g}(P)$ (ν_3), respectively. The position of bands suggested the octahedral geometry of Co(II) complex [21,22].

Nickel(II) complex shows a band with a maximum at 15,263 cm^{-1} which may be due to $^1A_1 \rightarrow {}^1A_2$ transition along with shoulder band at 17,892 cm^{-1} related to $^1A_1 \rightarrow {}^1B_1$ transition suggested the square planar geometry [21].

The electronic spectrum of Cu(II) complex displays four key bands. The bands at 32,144, 11,992, 17,374 and 26,057 cm^{-1} is due to charge transfer (L→M), $^2B_{1g} \rightarrow {}^2A_{1g}$ (ν_1), $^2B_{1g} \rightarrow {}^2B_{2g}$ (ν_2) and $^2B_{1g} \rightarrow {}^2E_{1g}$ (ν_3) transitions, which suggest the octahedral geometry of the Cu(II) complex [23,24].

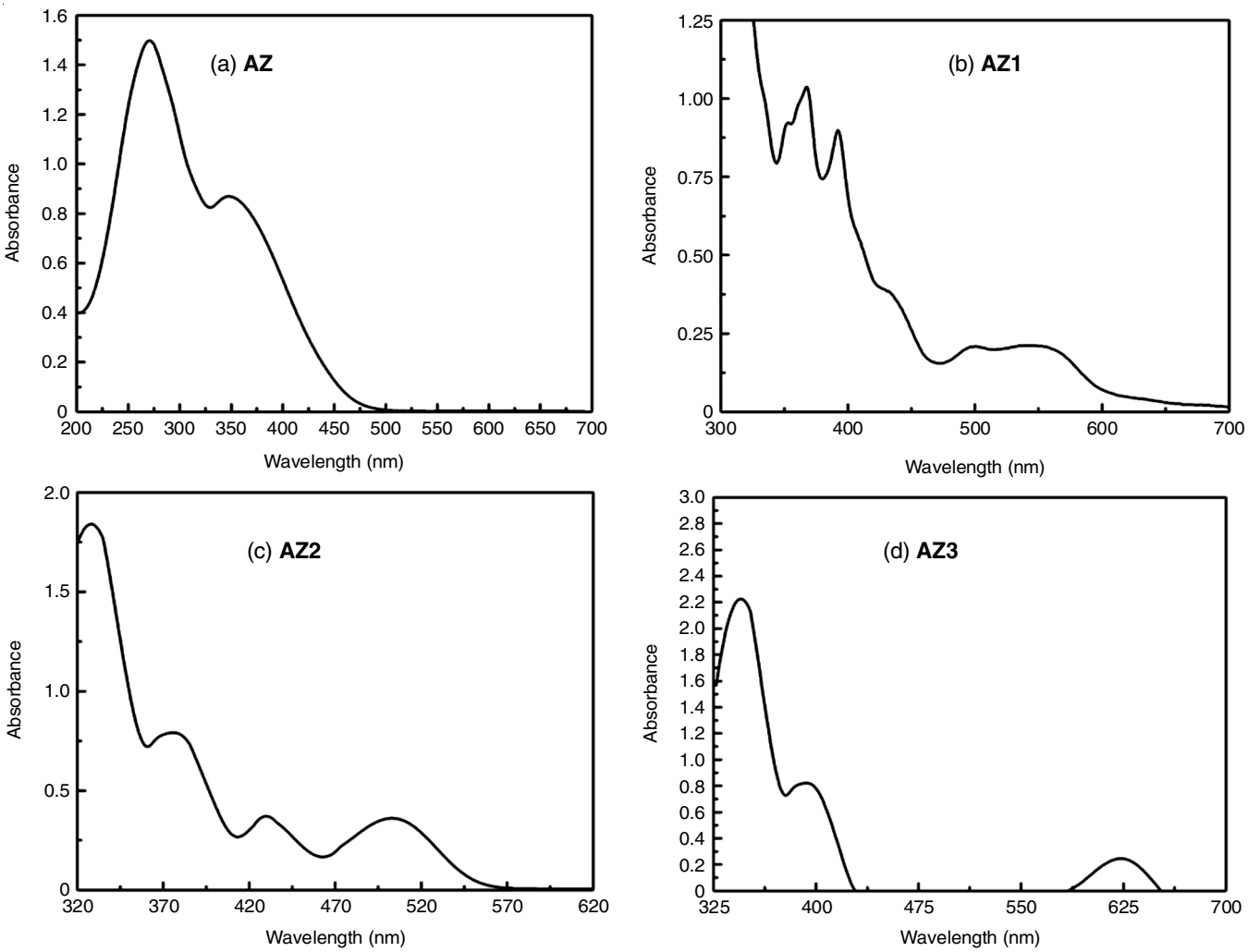

Fig. 7. Electronic spectra of **AZ** ligand and its metal complexes (**AZ1-AZ3**)

EPR analysis of Cu(II) complex: The EPR spectrum relayed to $[Cu(AZ)_2]$ (Fig. 8) be documented in normal temperature as solid crystal parts randomly oriented relative to each other (polycrystalline) sample, on X range of occurrence by 9.1 GHz in magnetic-field strength of 3000 g. The examination of $[Cu(AZ)_2]$ complex gives $g_{\parallel} = 2.182$, $g_{\perp} = 2.114$, $g_{av} = 2.088$ and G = 2.23. These g-values are being utilized to originate the ground state. In mixture octahedral geometry of $[Cu(AZ)_2]$, electrons that are not paired are present in the $d_{x^2-y^2}$ shells contributing $^2B_{1g}$ as the ground level with $g_{\parallel} > g_{\perp} > 2$, while electrons which were unpaired are present in d_{z^2} shells contributing $^2A_{1g}$ as ground level by $g_{\parallel} > g_{\perp} > 2$. In current cases, the $g_{\parallel} > g_{\perp} > 2$, therefore unpaired electrons present in $d_{x^2-y^2}$ orbital indicates an octahedral geometry that surrounded copper(II) ion [24]. It is moreover cross referred by attractive moment of $[Cu(AZ)_2]$ (1.83 BM), which confirms the mononuclear nature of complex. Orbital decline components, $K_{\parallel}$ and $K_{\perp}$ values which measured the spin-orbit pairing constant = 783 cm^{-1} for free copper (II) were obtained using Hathaway and Tomlinson *et al*. [25] and Stevens [26] methods. The $K_{\parallel}$ (0.68) and $K_{\perp}$ (0.74) components were determined by associations $K_{\parallel} = \alpha, \beta_1$ and $K_{\perp} = \alpha, \beta$, where α (0.74), β_1 (1.02) as well as β (1.09) are the coefficients of $d_{x^2-y^2}$, d_{xy} and d_{xz}, d_{yz} orbitals, which correspond to σ-bonding, in-plane π-bonding as well as away-from-plane bonding coefficients, respectively. By assuming, 1 = 1 (while ligand does not have accessible pair of bond on O atom which could bind to d_{xy}) the results of α and β were analyzed for $[Cu(AZ)_2]$.

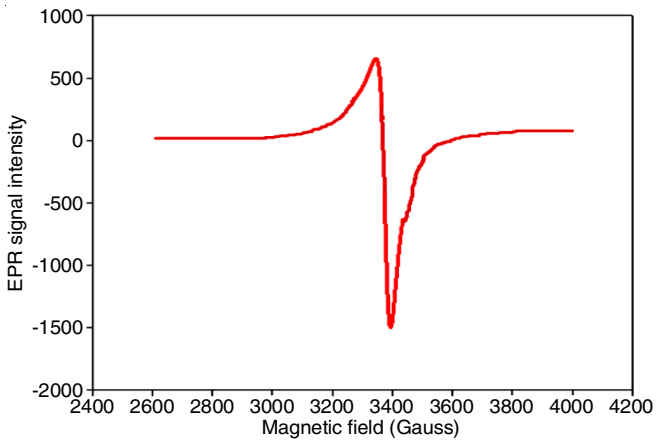

Fig. 8. EPR spectrum of $[Cu(AZ)_2]$ complex

Thermogravimetric analyses: The decomposition behaviour of the complexes (**AZ1-AZ3**) (Fig. 9) comprises three

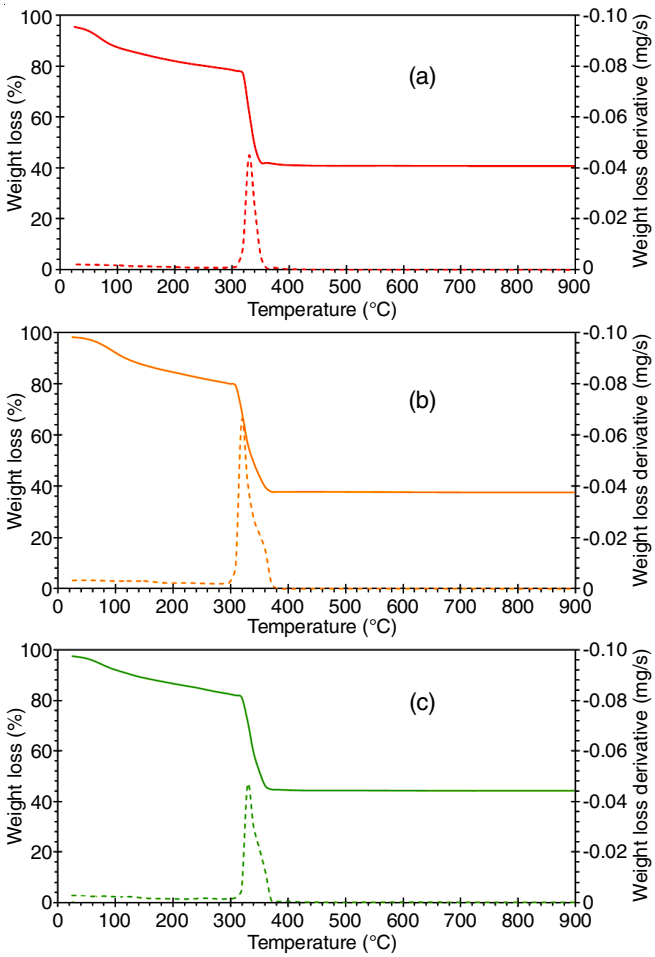

Fig. 9. Thermogravimetric curves of (a) **AZ1**, (b) **AZ2** and (c) **AZ3** complexes

degradation stages. The results of these measurements are listed in Table-3. The thermal decomposition of $[Cu(AZ)_2]$ complex showed 1st stage at 22-294 ºC with a mass loss of 36.52% (calcd. 36.88 %) due to removal of $C_{22}H_{12}N_3O$. The last step at 294-878 ºC with removal of 54.28% the total weight (calcd. 54.34%) corresponded to further decomposition of the organic ligand with production of CuO as final product.

For $[Co(AZ)_2]$ complex the 1st thermal step appeared at 23-298 ºC with mass loss 48.72% (calcd. 48.84%) is due to removal of $C_{30}H_{20}N_2O_2$. The 2nd stage occurred within 298-897 ºC with mass loss of 42.77% (calcd. 42.85%) and assigned to further decomposition of the organic moiety leading to the formation of CoO as ultimate product.

For $[Ni(AZ)_2]$ complex, the 1st step occurred at 260-303 ºC, is assigned to the evolution of $C_{24}H_{23}N_3O_2$ with a found mass

TABLE-3
THERMAL ANALYSIS DATA (TGA) OF THE METAL CHELATES

Complex	Temp. range (°C)	Mass loss (%)		Assignment
		Found	Calc.	
$[Cu(AZ)_2]$	22–294	36.52	36.88	Loss of $C_{22}H_{12}N_3O$.
	194–878	54.28	54.34	Further dissociation of the organic ligand with formation of CuO as final product
$[Co(AZ)_2]$	23–298	48.72	48.84	Loss of $C_{30}H_{20}N_2O_2$.
	457–897	42.77	42.85	Further dissociation of the organic ligand with formation of CoO as final product
$[Ni(AZ)_2]$	26–303	42.68	42.75	Loss of $C_{24}H_{23}N_3O_2$.
	203–889	48.87	48.96	Further dissociation of the organic ligand ($C_{28}H_{19}N_5O$) with formation of NiO as final product

loss of 12.11% (calcd. 12.14%). The last step within the temperature range of 303-889 ºC with weight loss of 44.52% (calcd. 44.56%) assigned to definitive degradation of the organic moiety leaving NiO as final residue.

Kinetic and thermodynamic parameters: Figs. 10-12 represent the Coats-Redfern [27] plots of the degradation stages of metal(II) complexes (**AZ1-AZ3**). The results shown in Table-4 concluded that (i) negative values of ΔS* indicate that a more ordered activated state or more rigid structure than the reactants or intermediates and the reactions are slower than ordinary state [28]; (ii) positive values of ΔH* were due to the endothermic decomposition processes [29]; (iii) high values of ΔE* supported the high stabilization of the studied complexes which is consequent of their covalent character [28]; and (iv) positive sign of ΔG* revealed the non-spontaneous decomposition processes [29].

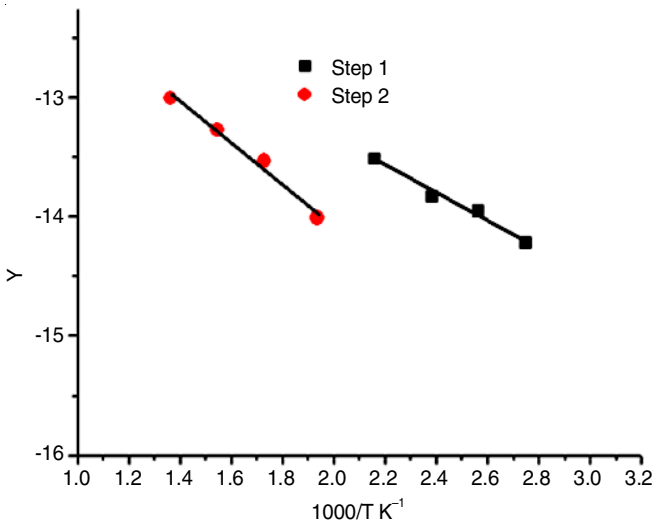

Fig. 10. Coats-Redfern plots for the decomposition steps of **AZ1**

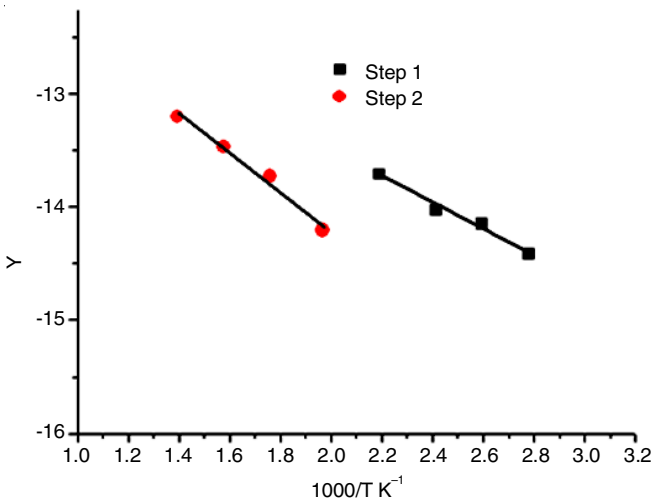

Fig. 11. Coats-Redfern plots for the decomposition steps of **AZ2**

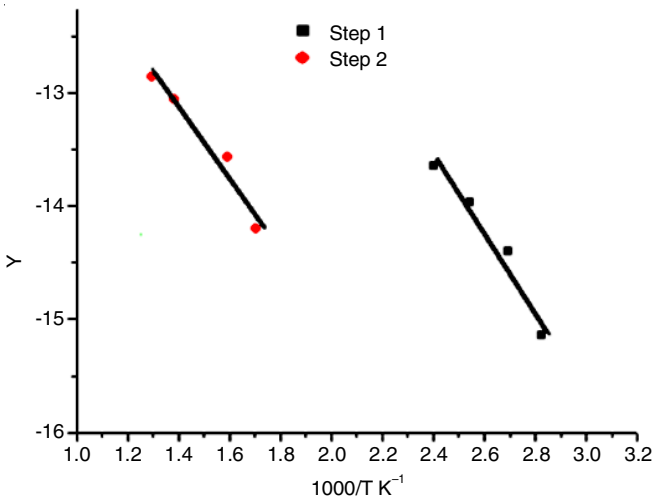

Fig. 12. Coats-Redfern plots for the decomposition steps of **AZ3**

XRD studies: The powder XRD patterns of complexes **AZ1-AZ3** were recorded over the 2θ = 2-80º range. The selected metal complexes exhibited a crystalline nature with sharp peaks (Fig. 13). The XRD unit cell parameters such as crystal nature, braves lattices, diffraction angles, cell length, volume, *etc*. are shown in Table-5. The XRD broad peaks at the bottom side in all the complexes indicate a smaller particle size which might be due to nanometer size. The average size of these complexes was calculated by Scherrer's formula [30]:

$$D = \frac{0.94\lambda}{\beta\cos\theta}$$

where λ is wavelength of X-ray radiation, β is the full width at half maximum (FWHM) of diffraction line and θ is the diffraction angle. The average crystallite sizes of all the complexes were found to be in nanometer scale.

SEM analysis: The SEM micrograph of all the metal complexes are shown in Fig. 14. The SEM micrograph taken in the three different scales 5 μm (A), 10 μm (B) and 20 μm (C). The synthesized metal complexes **AZ1-AZ3** shows be sponge, pod and rough rock ice of flower type shape respectively and the nanocrystalline sizes were 8.66, 4.82 and 14.18 nm. Complex **AZ1** shows stone shape nanoparticles with the presence of well in the stone, while the complex **AZ2** does not exhibit fine nano-

TABLE-4
TEMPERATURE OF DECOMPOSITION AND ACTIVATION PARAMETERS
(ΔH*, ΔS*, ΔG*) FOR DECOMPOSITION OF THE METAL CHELATES (**AZ1-AZ3**)

Complex	n	Step	r	T (K)	E*	ΔH*	A	-ΔS*	ΔG*
AZ1	0.66	1st	0.9989	478	62.456	53.698	1112546	0.20564	132.5642
	0.66	2nd	0.9997	793	51.368	46.663	1336984	0.12658	142.5356
AZ2	1	1st	0.9978	492	68.573	51.247	1135623	0.236558	120.6395
	1	2nd	0.9998	816	52.637	49.958	3045726	0.156854	132.5478
AZ3	1	1st	0.9899	484	46.358	43.159	1156246	0.188769	114.7534
	1	2nd	0.9996	832	53.129	52.587	2763578	0.179654	135.2419

TABLE 5
POWDER DIFFRACTION PARAMETERS OF THE COMPLEXES (**AZ1-AZ3**)

Complexes	**AZ1**	**AZ2**	**AZ3**
Empirical formula	$C_{52}H_{42}N_8O_4Ni$	$C_{52}H_{42}N_8O_4Co$	$C_{52}H_{42}N_8O_4Ni$
Formula weight	906.5	901.9	901.7
Crystal colour	Faint brown	Blue	Dark blue
Temperature (K)	298	298	298
Wavelength (Å)	1.54051	1.54051	1.540598
Radiation	Cu Kα	Cu Kα	Cu Kα
Crystal system	Orthorhombic (I)	Monoclinic (P)	Monoclinic (I)
a (Å)	14.50	8.44	7.91
b (Å)	17.72	11.77	7.06
c (Å)	18.38	4.77	10.07
α (°)	90	90	90.00
β (°)	90	93	101.3
γ (°)	90	90	90
a/b	0.7449	0.7757	1.4263
c/b	0.5245	0.6056	1.1204
Volume ($Å^3$)	562	474.11	551.45
Dx (g/cm^3)	1.591	1.509	1.87

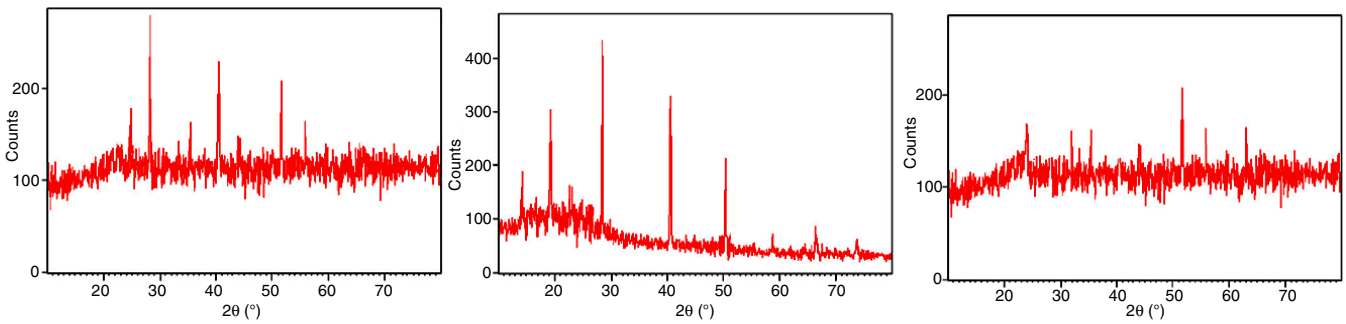

Fig. 13. XRD patterns of (a) copper complex; (b) nickel complex and (c) cobalt complex, respectively

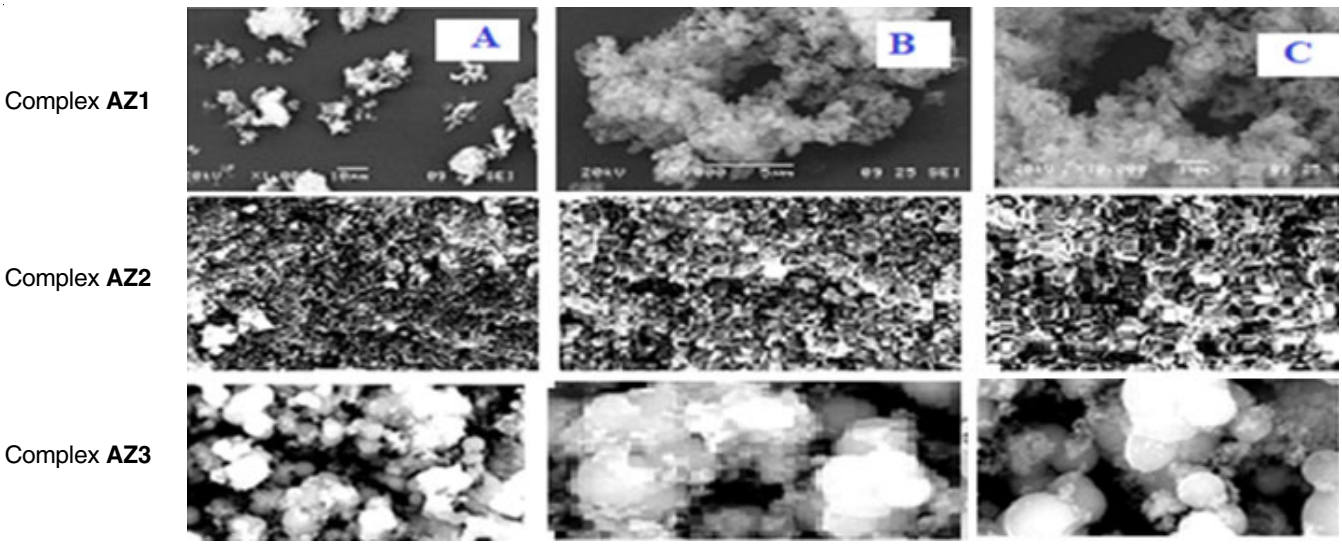

Fig. 14. SEM micrographs of the synthesized metal complexes (**AZ1-AZ3**)

particles. The complex **AZ3** shows spherical and aggumlation type shape.

Antimicrobial activity: All the synthesized complexes **AZ1-AZ3** were tested for their antibacterial and antifungal activities The obtained results are tabulated in Table-6. On the basis of inhibition zone diameter, it is clear that against *A. flavus*, azo-dye ligand and its metal complexes were found to be inactive. With respect to *C. albicans*, complex **AZ2** exhibits moderate efficiency (11 mm) while complex **AZ3** had weak antimicrobial efficacy (7 mm). It was also noticed that the metal complexes exhibited narrow inhibition zone for *S. aureus* as compared to the free ligand (14 mm). A variation in the activity of different

TABLE-6
DIAMETERS OF INHIBITION ZONES (mm) DISPLAYED BY THE LIGAND AND IT CHELATES CONTRA VARIOUS MICROORGANISMS

Compound	Inhibition zone diameter (mm/mg sample)			
	Escherichia coli (Gram-negative)	*Staphylococcus aureus* (Gram-positive)	*Aspergillus flavus* (Fungus)	*Candida albicans* (Fungus)
Azo-dye ligand (**AZ**)	12	14	0	0
Complex **AZ1**	12	8	0	0
Complex **AZ2**	8	6	0	11
Complex **AZ3**	8	11	0	7
Tetracycline (Antibacterial agent)	30	28	–	–
Amphotericin B (Antifungal agent)	–	–	17	18

compounds against various organisms relay either on variations in ribosome in microbial cells or the impermeability of cells of microbes. On the other hand, the prospective explication for the low efficacy of the metal complexes compared to the Schiff base compound may be caused due to (i) their disability to coordinate metals principle for the metabolism of microorganisms and/or to form hydrogen bonds with the active cites of cell structures, or (ii) low lipophilicity of the metal complexes compared with azo-dye ligand, where the permeation of compound through the lipid membrane is diminished [31,32].

Conclusion

Three novel complexes of Cu(II), Co(II) and Ni(II) with azo dye ligand have been synthesized and structurally characterized. Based on elemental analysis, molar conductivity, UV-visible, mass, ^{1}H and ^{13}C NMR, magnetic, ESR, FT-IR and thermal analysis data, mononuclear octahedral geometry of the general formula $[M(AZ)_2]$; (M = Cu(II), Co(II) and Ni(II) and AZ = ligand) is assigned. The molecular modeling studies confirmed the deduced geometrical arrangement of the metal chelates. The thermo-kinetic parameters have been also computed. The interaction mode of the investigated complexes with CT-DNA was examined *via* the absorption and viscosity techniques. The estimated binding constants for the DNA-complexes were $5.66 \pm 0.03 \times 10^4$, $2.02 \pm 0.03 \times 10^5$ and $3.42 \pm 0.03 \times 10^4$ M^{-1} for Co(II), Cu(II) and Ni(II) complexes, respectively. The calculated binding constant of the complexes follows the order Ni(II) > Co(II) > Cu(II). Evaluation of the viscosity change of CT-DNA upon increasing the complexes concentration indicated a negligible or small changes on the relative viscosity of DNA compared with ethidium bromide supporting a partial or non-intercalative binding mode for these compounds with DNA. This order stated that Ni(II) complex was more intensively bound to DNA. The antimicrobial efficiencies of the compounds have been checked contra various kinds of bacteria and fungi strains. The results showed that the tested compounds have low to moderate antimicrobial activity in comparison to standard drugs.

ACKNOWLEDGEMENTS

This research project was supported by a grant sanction from Research Center of the Female Scientific and Medical Colleges, Deanship of Scientific Research, King Saud University, Riyadh, Saudi Arabia

CONFLICT OF INTEREST

The authors declare that there is no conflict of interests regarding the publication of this article.

REFERENCES

1. E. Yildiz, M. Keles, A. Kaya and S. Dincer, *Chem. Sci. Trans.*, **2**, 547 (2013); https://doi.org/10.7598/cst2013.353
2. S.J. Naik and U.P. Halkar, *ARKIVOC*, 141 (2005); https://doi.org/10.3998/ark.5550190.0006.d12
3. H.R. Maradiya and V.S. Patel, *J. Braz. Chem. Soc.*, **12**, 710 (2001); https://doi.org/10.1590/S0103-50532001000600004
4. S.B. Savvin, V.P. Dedkova and O.P. Shvoeva, *Russ. Chem. Rev.*, **69**, 187 (2000); https://doi.org/10.1070/RC2000v069n03ABEH000538
5. J. Athira, Y. Sindhu, S. Sujamol and K. Mohanan, *J. Serb. Chem. Soc.*, **76**, 249 (2011); https://doi.org/10.2298/JSC100414025A
6. G.G. Mohamed, E.M. Zayed and A.M.M. Hindy, *Spectrochim. Acta A, Mol. Biomol. Spectrosc.*, **145**, 76 (2015); https://doi.org/10.1016/j.saa.2015.01.129
7. B. Padmashali, V.P. Vaidya, K.M. Mahadevan and K.P. Latha, *Indian J. Chem.*, **44B**, 1446 (2005).
8. P.K. Sharma, R.N. Khanna, B.K. Rohatgi and R.H. Thomson, *Phytochemistry*, **27**, 632 (1988); https://doi.org/10.1016/0031-9422(88)83161-3
9. G.K. Nagaraja, G.K. Prakash, M.N. Kumaraswamy, V.P. Vaidya and K.M. Mahadevan, *ARKIVOC*, 160 (2006); https://doi.org/10.3998/ark.5550190.0007.f19
10. M.N. Kumaraswamy and V.P. Vaidya, *Indian J. Heterocycl. Chem.*, **14**, 193 (2005).
11. Z.H. Chohan and C.T. Supuran, *J. Enzyme Inhib. Med. Chem.*, **23**, 240 (2008); https://doi.org/10.1080/14756360701474913
12. R. Ramesh and M. Sivagamasundari, *Synth. React. Inorg. Met.-Org. Chem.*, **33**, 899 (2003); https://doi.org/10.1081/SIM-120021656
13. H.A. Flaschka, EDTA Titration, Pergamon Press, edn 2 (1964).
14. A.I. Vogel, Textbook of Quantitative Inorganic Analysis, Longman: London, edn 4 (1978).
15. A. Vogel, Textbook of Practical Organic Chemistry, Longman Group: London, edn 5 (1989).
16. A.W. Bauer, W.M. Kirby, J.C. Sherris and M. Turck, *Am. J. Clin. Pathol.*, **45(4_ts)**, 493 (1966); https://doi.org/10.1093/ajcp/45.4_ts.493
17. W. Geary, *Coord. Chem. Rev.*, **7**, 81 (1971); https://doi.org/10.1016/S0010-8545(00)80009-0
18. P. Tyagi, S. Chandra, B.S. Saraswat and D. Sharma, *Spectrochim. Acta A*, **143**, 1 (2015); https://doi.org/10.1016/j.saa.2015.02.027
19. P. Tyagi, S. Chandra and B.S. Saraswat, *Spectrochim. Acta A, Mol. Biomol. Spectrosc.*, **134**, 200 (2015); https://doi.org/10.1016/j.saa.2014.06.112

20. H.A. Bayoumi, A.M.A. Alaghaz and M.S. Aljahdali, *Int. J. Electrochem. Sci.*, **8**, 9399 (2013).
21. M. Tyagi, S. Chandra and P. Tyagi, *Spectrochim. Acta A, Mol. Biomol. Spectrosc.*, **117**, 1 (2014); https://doi.org/10.1016/j.saa.2013.07.074
22. J.C. Bailar, H.J. Emeleus, R. Nyholm and A.F. Trotman-Dickenson, Comprehensive Inorganic Chemistry, Pergamon Press, vol. 3 (1975).
23. F.A. Cotton and G. Wilkinson, Advanced Inorganic Chemistry: A Comprehensive Text, John Wiley & Sons: New York, edn 4 (1986).
24. N. Kavitha and P.V.A. Lakshmi, *J. Mol. Struct.*, **1176**, 798 (2019); https://doi.org/10.1016/j.molstruc.2018.09.042
25. B.J. Hathaway and A.A.G. Tomlinson, *Coord. Chem. Rev.*, **5**, 1 (1970); https://doi.org/10.1016/S0010-8545(00)80073-9
26. K.W.H. Stevens and and M.H.L. Pryce, *Proc. Roy. Soc. (London)*, **A219**, 542 (1953); https://doi.org/10.1098/rspa.1953.0166
27. A.W. Coats and J.P. Redfern, *Nature*, **201**, 68 (1964); https://doi.org/10.1038/201068a0
28. W. Wendland, Thermal Methods of Analysis, Interscience: New York, vol. XIX, pp. 424 (1964).
29. J.K. Basu, M. Shannigrahi, N. Ray and S. Bagchi, *Spectrochim. Acta A, Mol. Biomol. Spectrosc.*, **61**, 2539 (2005); https://doi.org/10.1016/j.saa.2004.09.017
30. P. Scherrer, *Göttinger Nachrichten Gesell.*, **2**, 98 (1918).
31. F. Yakuphanoglu, I. Erol, Y. Aydogdu and M. Ahmedzade, *Mater. Lett.*, **57**, 229 (2002); https://doi.org/10.1016/S0167-577X(02)00771-1
32. V.A. Kawade, A.A. Kumbhar, A.S. Kumbhar, C. Näther, A. Erxleben, U.B. Sonawane and R.R. Joshi, *Dalton Trans.*, **40**, 639 (2011); https://doi.org/10.1039/C0DT01078B